energies

MDPI

Article

Nonlinear Model Predictive Control of Heaving Wave Energy Converter with Nonlinear Froude–Krylov Forces

Tania Demonte Gonzalez [1,*,†], Enrico Anderlini [2,†], Houssein Yassin [1,†] and Gordon Parker [1,†]

[1] Mechanical Engineering–Engineering Mechanics Department, Michigan Technological University, Houghton, MI 49931, USA; hyassin@mtu.edu (H.Y.); ggparker@mtu.edu (G.P.)
[2] Department of Mechanical Engineering, University College London, London WC1N 1AX, UK; e.anderlini@ucl.ac.uk
* Correspondence: tsdemont@mtu.edu
† These authors contributed equally to this work.

Abstract: Wave energy holds significant promise as a renewable energy source due to the consistent and predictable nature of ocean waves. However, optimizing wave energy devices is essential for achieving competitive viability in the energy market. This paper presents the application of a nonlinear model predictive controller (MPC) to enhance the energy extraction of a heaving point absorber. The wave energy converter (WEC) model accounts for the nonlinear dynamics and static Froude–Krylov forces, which are essential in accurately representing the system's behavior. The nonlinear MPC is tested under irregular wave conditions within the power production region, where constraints on displacement and the power take-off (PTO) force are enforced to ensure the WEC's safety while maximizing energy absorption. A comparison is made with a linear MPC, which uses a linear approximation of the Froude–Krylov forces. The study comprehensively compares power performance and computational costs between the linear and nonlinear MPC approaches. Both MPC variants determine the optimal PTO force to maximize energy absorption, utilizing (1) a linear WEC model (LMPC) for state predictions and (2) a nonlinear model (NLMPC) incorporating exact Froude–Krylov forces. Additionally, the study analyzes four controller configurations, varying the MPC prediction horizon and re-optimization time. The results indicate that, in general, the NLMPC achieves higher energy absorption than the LMPC. The nonlinear model also better adheres to system constraints, with the linear model showing some displacement violations. This paper further discusses the computational load and power generation implications of adjusting the prediction horizon and re-optimization time parameters in the NLMPC.

Keywords: wave energy converter; optimization; point absorber; marine energy; nonlinear control; model predictive control; nonlinear model predictive control

Citation: Demonte Gonzalez, T.; Anderlini, E.; Yassin, H.; Parker, G. Nonlinear Model Predictive Control of Heaving Wave Energy Converter with Nonlinear Froude–Krylov Forces. *Energies* **2024**, *17*, 5112. https://doi.org/10.3390/en17205112

Academic Editors: Umesh A. Korde and Michael E. McCormick

Received: 18 September 2024
Revised: 8 October 2024
Accepted: 9 October 2024
Published: 15 October 2024

1. Introduction

Water waves are predictable and carry a high content of energy; yet, they represent the world's largest underutilized renewable energy resource. Ocean waves have the potential to meet the demand for energy with an estimated power of 2300 TWh/year in the United States, equivalent to 57% of the electricity generated in 2019 [1]. Despite the resource potential, marine energy technologies, especially wave energy converters (WECs), are still in the early stage of development and will require further research to become economically competitive in the energy market [2].

One of the main objectives in wave energy converters research nowadays is to find ways of reducing their levelized cost of energy (LCOE), which is defined as the ratio of the total capital expenditures (CAPEX) and operational expenditures (OPEX) to the total energy produced over the system's lifetime. Therefore, to reduce the LCOE is necessary to (1) decrease the capital and operational expenditures and (2) increase the annual energy

production (AEP) [3]. Advancing the control strategies to maximize the energy capture of WECs has shown the potential to increase the WEC AEP by up to 197% [4] and, therefore, lower their LCOE.

Many different wave energy converter devices can be found in the literature, but their main working principle is the same: transform the energy of waves into useful forms of energy through the Power Take-Off system (PTO). The authors in [5,6] present a review and classification of wave energy converter technologies. Because of their simplicity, and capabilities offshore, this paper focuses on spherical single-body heaving point absorber (HPA) wave energy converters.

When designing model-based control strategies, it is crucial to have an accurate mathematical model of the system. HPAs are most commonly modeled using a linear approach based on the Cummins equation [7]. This model is simple and computationally convenient when small motions are considered. However, when control strategies are applied through the PTO system to maximize power absorption, the motion of the WEC is exaggerated. As a result, the nonlinearities in the system become significant and must be considered to obtain an accurate WEC model [8]. To address these nonlinearities, this paper presents a nonlinear model predictive control (NLMPC) strategy and compares its performance to the widely used linear model predictive control (LMPC).

Model predictive control is an optimal control algorithm that uses the WEC mathematical model to predict the future behavior of the states over a finite prediction horizon and adjust the input to minimize the objective function [9]. An attractive feature of MPC is that it can be used with nonlinear models, and the optimal control solution can be subjected to constraints of the states and the input. In addition to MPC, various optimal control strategies have been developed to enhance the performance of WECs. Ringwood et al. provides a comprehensive review of these approaches in [10]. Similarly, extensive research has been conducted on MPC for wave energy converters. However, most of the literature focuses on LMPC, while only a few authors focus on NLMPC strategies. A comprehensive review of MPC in WECs suggests that less than 15% of articles consider NLMPC algorithms [11].

MPC is an established control strategy in industrial processes [9], which suggests a great potential for WEC applications. The authors in [12] were one of the first researchers to propose using NLMPC to deal with nonlinearities in WECs. The WEC was a floating 2-body HPA with nonlinear mooring forces. The results showed that using NLMPC yielded better outcomes for certain wave conditions; however, for others, using NLMPC over LMPC was not justifiable. A subsequent study [13] based on the same mooring configuration used an extended Kalman filter to estimate the states of the WEC, resulting in a 53% improvement in the computational effort. Both articles paved the way for the development of NLMPC by incorporating nonlinear mooring forces. However, in this paper, a fixed spherical HPA is considered, where the most significant nonlinear terms are given by the Froude–Krylov (FK) forces [14].

Guang Li [15] proposed a NLMPC of a WEC based on differential flatness parameterization, which incorporates the nonlinear buoyancy force of a non-uniform cross-sectional area buoy. The results showed an improvement in the computational effort when using flatness parameterization with a NLMPC. These results are heavily focused on the computational performance of the algorithm and not so much on the energy maximization of the control law. A more recent study [16] presented a NLMPC strategy based on the real-time iteration scheme. The nonlinear term is given by the incorporation of the PTO system efficiency; however, the WEC model is a linearized system. The focus of this paper is not on real-time applicability but rather on the energy maximization of a nonlinear WEC model with significant nonlinear forces.

In the literature, different NLMPC strategies have been developed with an objective in mind: reducing the LCOE by increasing energy production. Therefore, the structure of the NLMPC algorithm is very similar in most of the articles. The common objective function, which is also adopted in this study, is the energy maximization over a finite prediction horizon while complying with constraints. The constraints are more commonly applied to

the amplitude of the motion, the velocity of the floating device, and the maximum force of the PTO system. The NLMPC algorithm optimizes the power generated by manipulating the PTO force over the finite prediction horizon.

WEC control systems, contrary to traditional control systems that aim to reject disturbances, must exploit wave forces to maximize energy extraction. Thus, knowing the wave forces, over the prediction horizon, helps with the implementation of a WEC MPC solution. Methods such as Kalman filters, autoregressive models, and neural networks have been employed to forecast these forces [17–19]. This study presumes perfect knowledge of future wave elevations for the control horizon to focus on control strategy differences between LMPC and NLMPC without the wave force prediction complication.

The literature has shown the potential of MPC algorithms to improve the performance of WECs, and, therefore, it is crucial to keep investigating and improving the WEC models and control algorithms to advance the technology. This paper presents an NLMPC algorithm employing a nonlinear Froude–Krylov force model with a fidelity of 0.91–0.97, subjected to realistic force constraints, comparing its efficacy against a linearized model over various prediction horizons and optimization times. This article is based on Chapter 6 of the author's PhD thesis [20].

The content of the paper is organized as follows: Section 2 describes the linear and nonlinear WEC mathematical models used in the analysis of the MPC performance. Section 3 describes the MPC algorithm and the details of the optimization statement, Section 4 shows the results and discussion on the performance of the control strategy, and finally, Section 5 contains the conclusion.

2. Wave Energy Converter Modeling

Mathematical models for WECs are crucial for developing model-based control systems. Typically, these models are linear due to their lower computational demands, operating under the assumption of small displacements. However, there are scenarios where the device experiences significant motion while still generating power, making the nonlinear characteristics increasingly relevant. This work specifically addresses these scenarios.

As illustrated in Figure 1, a heaving buoy is connected to a PTO system anchored to the seabed. The incoming waves $\eta(t)$ produce vertical oscillations in the buoy, creating a relative velocity between the floating body and the submerged plate. This interaction enables the conversion of kinetic energy into electrical energy. Assuming an incident flow that is inviscid, irrotational, and incompressible, the general hydrodynamic model for a heaving WEC is described as follows:

$$m\ddot{z}(t) = F_{FK_{st}} + F_{FK_{dy}} + F_g + F_D + F_R + F_{PTO} \tag{1}$$

where m is the dry mass of the buoy, $z(t)$ is the displacement of the buoy from equilibrium, $F_{FK_{st}}$ and $F_{FK_{dy}}$ are the hydrostatic and hydrodynamic Froude–Krylov forces, respectively, F_g is the gravitational force, F_D is the diffraction force, F_R is the radiation force, and F_{PTO} is the PTO force.

As the incoming wave field interacts with the buoy, the waves bend around the edges of the structure, a phenomenon known as the diffraction force F_D. When the diameter of the buoy is much smaller than the length of the wave, the diffracted waves from the buoy become insignificant and can, therefore, be safely disregarded [21].

The radiation force is exerted on the body as it oscillates in undisturbed water, and it is expressed as

$$F_R = -m_\infty \ddot{z}(t) - \int_{-\infty}^{\infty} K_R(t-\tau)\dot{z}(\tau)d\tau \tag{2}$$

which contains the inertial term represented by the added mass at infinite frequency m_∞ and the radiation convolution term where K_R is the radiation impulse response function kernel. Solving this convolution integral is computationally demanding; therefore, to increase the computational speed and to facilitate the use of conventional control methods,

the radiation convolution is approximated by a state-space model [8]. The linear system is described as

$$\dot{X}_R(t) = \mathbf{A_R} X_R(t) + \mathbf{B_R} u(t); \;\; X_R(0) = 0$$
$$\int_0^t K_R(t-\tau)d\tau \approx \mathbf{C_R} X_R(t) + \mathbf{D_R} u(t)$$

where $\mathbf{A_R}$ and $\mathbf{B_R}$ are the state space matrices, and the output state space matrices are $\mathbf{C_R}$, $\mathbf{D_R}$. The input to the system represented by u is the velocity of the buoy, and X_R is the state vector describing the convolution kernel K_R. Figure 2 shows the agreement between the kernel and a 3rd-order state-space approximation. The frequency-dependent parameters of the buoy as well as the radiation state space model values are listed in Table 1.

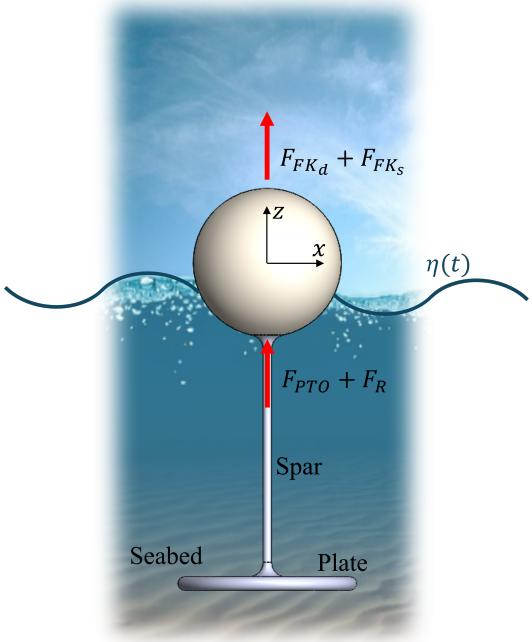

Figure 1. Illustration of a spherical heaving point absorber (HPA) wave energy converter.

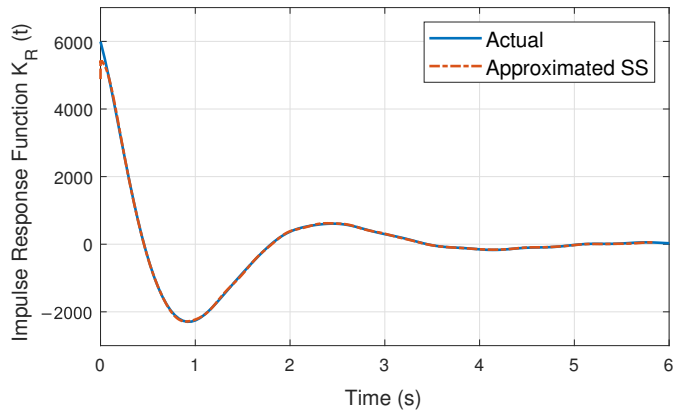

Figure 2. Actual and approximated radiation impulse response function.

Table 1. Spherical buoy parameters.

Parameter	Values
WEC radius R	2.5 m
WEC mass m	32,725 kg
WEC draft h_0	2.5 m
Added mass A_∞	14,019 kg
Natural Frequency ω_n	2 rad/s
Radiation damping A_r	$\begin{bmatrix} -1.74 & -2.39 & -0.23 \\ 1 & 0 & 0 \\ 0 & 1 & 0 \end{bmatrix}$
Radiation damping B_r	$\begin{bmatrix} 1; & 0; & 0 \end{bmatrix}$
Radiation damping C_r	$\begin{bmatrix} -2.39 \times 10^4 & -2.1 \times 10^3 & 0 \end{bmatrix}$
Radiation damping D_r	0

2.1. Nonlinear Froude–Krylov Force

The heaving point absorber's primary nonlinear hydrodynamic force component is the Froude–Krylov force F_{FK} [14,22]. This force is obtained from integrating the pressure resulting from the incoming waves across the wetted surface. It combines two forces: the hydrostatic force $F_{FK_{st}}$ and the hydrodynamic force $F_{FK_{dy}}$. The FK hydrostatic force is the net force resulting from the difference between the force due to gravity F_g and the buoyancy force. In terms of pressure, $F_{FK_{st}}$ is defined as the difference between F_g and the force exerted by the hydrostatic pressure acting on the buoy's wetted surface. In contrast, the FK hydrodynamic force $F_{FK_{dy}}$ is calculated by integrating the unsteady pressure field induced by the incident waves over the buoy's wetted surface. Combining the two components, the FK force can be mathematically expressed as

$$F_{FK} = F_g - \int_0^{2\pi} \int_{\sigma_1}^{\sigma_2} P(z,t) f'(\sigma) f(\sigma) d\sigma d\theta \tag{3}$$

where the integrals take into consideration the profile of revolution of the shape of the device $f(\sigma)$ and the total pressure experienced by the buoy $P(z,t)$. Assuming that this is an offshore WEC, the pressure exerted on the buoy by the waves can be obtained by Airy's wave theory [23] for deep water waves:

$$P(z,t) = \rho g \sum_{i=1}^{n} e^{\chi_i z} \eta_i - \rho g z \tag{4}$$

where

$$\eta_i = A_i \sin(\phi_i - \omega_i t) \tag{5}$$

such that A_i is the wave amplitude component, ϕ_i is the phase shift, χ_i is the wave number, and ω_i is the angular frequency. Using Equation (5), the time series irregular wave elevation can, thus, be expressed as $\eta(t) = \sum_{i=1}^{n} \eta_i$.

In linear models, where small displacements are assumed, the Froude–Krylov (FK) force is integrated over the mean wetted surface of the buoy. In contrast, the nonlinear approach accounts for the instantaneous wetted surface, which typically demands significantly more computational resources. However, Giorgi et al. [24] introduced a computationally efficient algebraic solution that is derived by integrating the pressure over the profile of revolution of the device considering the instantaneous wetted surface area. This paper incorporates the nonlinear FK force model developed and validated in [20], where the author built upon the methodology originally employed by Giorgi et al. to derive closed-form expressions for the FK forces. This modified approach extends beyond previous scopes by redefining the profile of revolution of the buoy shape and the limits of integration to (1) accommodate for varying drafts of the buoy and (2) satisfy the dynamic boundary condition in Airy's theory.

To account for the instantaneous wetted surface area of the spherical buoy up to the still water level, the profile of revolution $f(\sigma)$ as well as the limits of integration σ_1 and σ_2 are redefined as [25]:

$$f(\sigma) = \sqrt{R^2 - (-R + h_0 - z(t) + \eta(t) + \sigma)^2} \tag{6}$$

where R is the radius of the sphere, h_0 is the draft of the buoy, and σ is the integral variable that defines the limits of integration as

$$\begin{cases} \sigma_1 = -h_0 + z(t) - \eta(t) \\ \sigma_2 = 0 \end{cases} \tag{7}$$

Solving the integral term of the FK force in Equation (12) and separating the FK force into the hydrostatic and hydrodynamic force, the resulting nonlinear forces are

$$F_{FK_s} = F_g - 2\pi\rho g \int_{\sigma_1}^{0} \sigma(R - h_0 + z(t) - \eta(t) - \sigma)d\sigma \tag{8}$$

$$F_{FK_d} = 2\pi\rho g \int_{\sigma_1}^{0} \sum_{i=1}^{n} (e^{\chi_i z} A_i cos(\omega_i t + \phi_i))(R - h_0 + z(t) - \eta(t) - \sigma)d\sigma \tag{9}$$

When considering the fidelity of this model, this method classifies as partially nonlinear, providing high accuracy at low computational costs.

2.2. Wave Spectrum

The wave characteristics used in this paper were chosen based on realistic wave conditions across different wave energy test sites across the United States. The most common ocean spectra used to model irregular waves are the Bretschneider, Pierson–Moskowitz (PM), and JONSWAP spectra. In this study, the PM spectrum was used.

The two-parameter PM spectrum can be obtained from the significant wave height H_{m0} and the peak wave frequency f_p. The range of H_{m0} and energy periods T_e are chosen based on the occurrence of each sea state and its contribution to wave energy. For example, at the U.S. Navy Wave Energy Test Site (WETS) in Hawaii, the most frequent sea states occur within the range of 1 m $< H_{m0} <$ 2.5 m and 5 s $< T_e <$ 11 s [26]. However, these sea states do not always contribute the most wave energy. In an average year, the total wave energy in this location is 125,850 kWh/m, and the wave characteristics that contribute the most energy are within the range of 1.5 m $< H_{m0} <$ 2 m and 7 s $< T_e <$ 8 s.

The PM spectrum was computed using the wecSim tool [27]. The spectral density of the surface elevation defined by the PM spectrum [28] is defined by

$$S(f) = \frac{(H_{m0})^2}{4}(1.057 f_p)^4 f^{-5} exp(-\frac{5}{4}(\frac{f_p}{f})^{-4}) \tag{10}$$

where $A = 0.675$ is a nondimensional constant and $\omega_s = T_p/1.167$ is the significant frequency associated with the peak period. Figure 3 shows a PM spectrum and the time series wave elevation generated using random phases ϕ, described as

$$\eta(t) = \sum_{i=1}^{n} A_i \cos(\omega_i t + \phi_i) \tag{11}$$

where n is the number of wave components, ω_i is each component's wave frequency, and the wave amplitudes are obtained from the wave spectrum as $A_i = \sqrt{2S(\omega_i)\, d\omega_i}$.

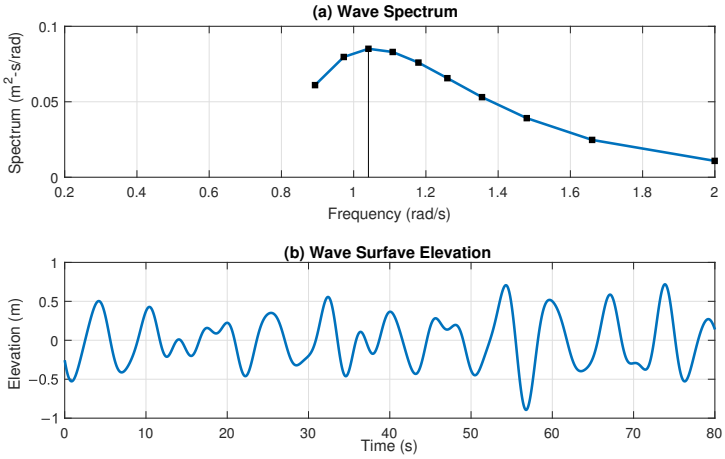

Figure 3. (**a**) Pierson–Moskowitz spectrum and (**b**) the wave elevation profile for a wave of T_p = 6 s and H_{m0} = 1 m described with $n = 10$ wave components.

3. Model Predictive Control

Model predictive control (MPC) leverages the WEC mathematical model to predict the future behavior of the system over a finite prediction horizon. It optimizes performance by fine-tuning the inputs to the system. This strategy is particularly advantageous as it can manage constraints on system states and inputs while incorporating predictions of external inputs. The main components of MPC include a precise prediction model, an objective function to guide performance metrics, defined system constraints, and an optimization algorithm to seek the best control actions.

For optimizing the performance of wave energy converters, two primary approaches are typically employed. The first approach centers on minimizing the error between an optimal velocity reference and the actual velocity of the WEC while complying with the constraints. This approach requires having an optimal trajectory. In linear WEC models subjected to regular waves, the optimal velocity trajectory can be defined by

$$|\dot{z}^*(\omega)| = \frac{|F_{FK_d}(\omega)|}{2B(\omega)} \tag{12}$$

where $B(\omega)$ is the radiation damping coefficient. However, this optimal trajectory requires large motions and large forces, making the solution impractical. Moreover, for nonlinear WEC models under irregular wave conditions, deriving an explicit optimal velocity reference becomes significantly more challenging. Given these complexities, this study explores a second approach: maximizing the power output of the WEC while adhering to motion and force constraints. This method offers a more direct and potentially more feasible way to enhance WEC efficiency under varying operational conditions.

The MPC algorithm requires a discrete function of the model. Combining the equations described in Section 2, the discrete WEC model can be represented in the general discrete form of

$$\begin{aligned} x_{k+1} &= f(x_k, F_{PTO_k}, \eta_k) \\ y_{k+1} &= g(x_k) \end{aligned} \tag{13}$$

where k represents the current time and x_k are the states of the system $[z; \dot{z}; X_R]$ at time k, and y_k are the outputs of the system $[z; \dot{z}; X_R]$. Using these discrete system dynamics, the future behavior of the WEC can be predicted over a finite horizon of length N_h where the prediction horizon time is $T_h = N_h dt$. The predicted states of the system are as follows:

$$x_{k+1|k} = f(x_{k+i-1|k}, F_{PTO_{k+i-1}}, \eta_{k+i-1}), \quad i = 1, 2, ..., N_h \tag{14}$$

where $x_{k+i-1|k}$ denotes the predicted state of the system at time $k+i$ based on samples up to time k. The control objective is to find the optimal PTO force that optimizes the energy absorbed:

$$E_{absorbed} = -\sum_{i=k+1}^{k+N_h-1} F_{PTO_{i|k}} \dot{z}_{i|k} \tag{15}$$

Therefore, the cost function to be minimized can be formulated as

$$J = \sum_{0}^{N_h} F_{PTO_{i|k}} \dot{z}_{i|k} \tag{16}$$

By minimizing the negative of the absorbed energy, the total energy absorbed is maximized. This optimization problem is subject to the following two constraints:

$$\begin{aligned} \eta_k - z_{max} < |z_k| < \eta_k + z_{max} \quad k = 1, 2, ..., N_h \\ |F_{PTO_k}| < F_{PTO_{max}} \quad k = 0, 2, ..., N_h - 1 \end{aligned} \tag{17}$$

where z_{max} is the maximum relative displacement of the WEC. The constraints implemented in this work are listed in Table 2. Furthermore, previous research has shown that large incoming waves can lead to solution infeasibility [29]. To mitigate these infeasibilities, a penalty term is incorporated into the cost function:

$$J = \sum_{0}^{N_h} F_{PTO_{i|k}} \dot{z}_{i|k} + q/\Delta z_{i|k} \tag{18}$$

where $q > 0$ is the weighting factor for the position penalty term, and Δz represents the difference between the max or min displacement constraints and the actual displacement. This penalty term is only activated when the displacement is within 5% of the constraint limit. Thus, if the displacement is outside this 5% region, the weighting factor q is set to zero. The general form of the optimization problem can then be described mathematically as

$$\min_{F_{PTO}} \sum_{0}^{N_h} F_{PTO_{i|k}} \dot{z}_{i|k} + q/\Delta z_{i|k} \tag{19}$$

subject to the constraints in Equation (17).

At time step k, the optimization problem is solved to find the optimal parameters of the control input sequence F^*_{PTO}. Typically, this optimal control input is implemented until the next measurement becomes available and the optimization problem is solved again. However, this time difference between re-optimizations T_{opt} can vary [30]. In this study, different re-optimization times are used in the simulations to evaluate the control performance vs. simulation time. The prediction horizons T_h and re-optimization times T_{opt} used in the simulation are listed in Table 2. The obtained F^*_{PTO} sequence is implemented in the system until the next optimization step.

Table 2. Nonlinear MPC simulation parameters.

Parameter	Symbol	Value	Units
Displacement Limits	$[z_{min}, z_{max}]$	$[-2, 2]$	m
PTO Amplitude Limit	$F_{PTO_{max}}$	300	kN
Simulation Time Step	T_s	0.01	s
Controller Update Time	T_c	0.04	s
Prediction Horizon	T_h	6 and 12	s
Optimization Update Time	T_{opt}	3 and 6	s
Position Weighting Factor	q	100	-

In the literature on MPC, it is common to define a control horizon T_c over which the optimal control input is obtained using the predicted states of the system. In this paper, $T_c = T_h$; therefore, an optimal control input sequence is obtained for the entire prediction horizon. The workflow of the MPC algorithm used in this study is described in Figure 4.

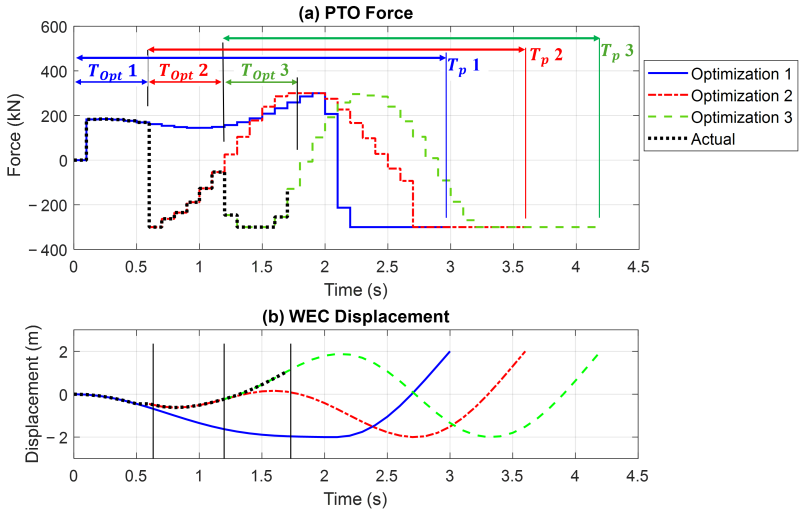

Figure 4. Model predictive control schedule where T_{h_i} is the prediction horizon of the i^{th} iteration, and T_{opt_i} is the optimization time horizon for the i^{th} iteration.

It is important to clarify that the focus of this study is not on real-time implementation. Instead, the emphasis is on assessing the qualitative performance of NLMPC in controlling a nonlinear WEC model characterized by nonlinear Froude–Krylov forces. This study aimed to determine whether the NLMPC offers advantages over the LMPC. Both controllers were implemented in MATLAB and Simulink Version 2024a, where the LMPC utilized the linearized model of Equations (8) and (9). For the NLMPC, the MATLAB solver "fmincon" was employed, capable of handling nonlinear dynamics with nonlinear constraints. The "sqp" method was chosen as the optimization algorithm for "fmincon" because of its strong convergence properties, robustness in handling complex nonlinearities, and effectiveness in managing inequality constraints. The linearized version of the FK forces was obtained using Taylor series expansion evaluated at $z = 0$ and $\eta = 0$. This was performed using the "taylor" command in MATLAB.

Figure 5 illustrates the model predictive controller schematic and how it incorporates the WEC model. In the simulation, the MPC operates using both linear and nonlinear models for comparative analyses, while the true model uses the nonlinear Froude–Krylov force.

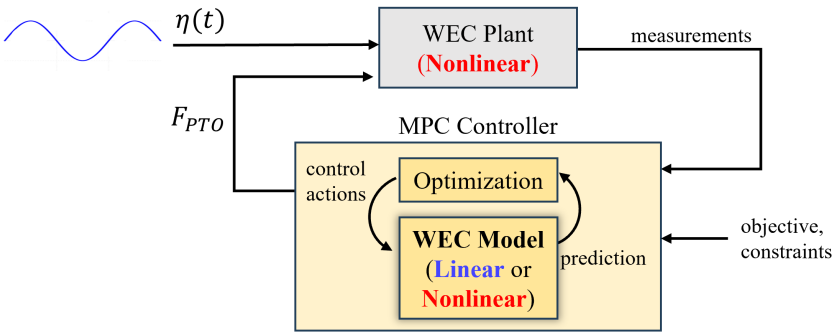

Figure 5. Model predictive controller schematic. Adapted from [31] licensed under CC BY-NC-ND 4.0.

4. Results and Discussion

In this study, the state prediction in the MPC was performed using both the actual nonlinear model of the WEC and a linear approximation. Both models were tested for a

range of irregular waves created using the PM spectrum in Equation (10) and constructing the irregular wave elevation profile in Equation (11) with 10 frequency components to form an 80-s duration wave elevation with random phases. In the simulation, different prediction horizons and re-optimization times were used. To evaluate how these parameters affect the performance of the WEC and the relevance of including the nonlinear forces, this section is divided into the following segments.

4.1. Linear vs. Nonlinear Model Comparison

Figure 6 shows the comparison of energy absorbed by the WEC, the PTO force, and the WEC displacement using the two models for a wave of H_s = 1.5 m and T_p = 6 s. From this figure, it is clear that the nonlinear model improves the performance of the WEC when compared to the linear model. Their respective power production was 37.3 kW with the linear prediction model and 54.5 kW with the nonlinear model, improving the performance by 46.1% over the linear model. This performance analysis was conducted for the range of waves tested with different prediction horizons and optimization times. The tables in Figure 7 show the percentage difference in power production between the nonlinear and linear MPC, which is calculated by

$$\% \text{ Power Difference} = \left(\frac{-(P_L - P_{NL})}{P_L} \right) \times 100\% \tag{20}$$

where P_L is the power produced by the linear MPC model, and P_{NL} by the nonlinear MPC model. The percentage difference quantitatively measures the extent to which the nonlinear model produces more or less power compared to the linear model. A negative percentage indicates a better performance of the linear MPC, and it is shaded in blue.

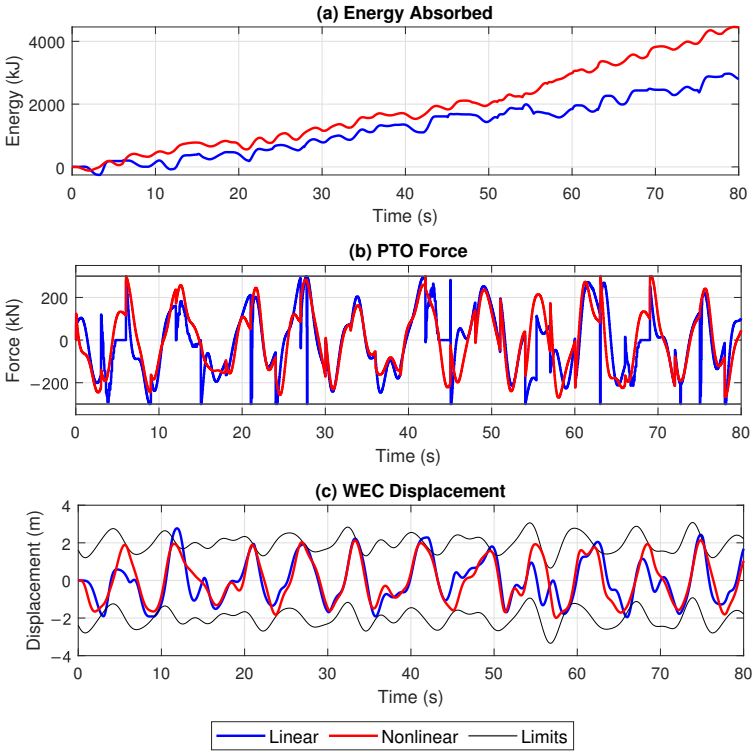

Figure 6. Energy absorbed and PTO force for a wave of H_s = 1.5 m and T_p = 6 s. The prediction horizon and optimization times are 6 s and 3 s, respectively.

By observing the performance comparison between linear and nonlinear MPC across several wave conditions in Figure 7, it is evident that the overall performance is improved by incorporating the nonlinearities into the predictive model. This is particularly clear

at lower wave periods for an optimization time T_{opt} = 3 s as shown in Figure 7a,c. For instance, at a wave energy period of 6 s, the NLMPC shows a performance improvement of up to 46%. However, looking at the same optimization time of 3 s but at higher wave periods, the performance difference reduces, and in the case of the wave at a 9 s period and a height of 1.5 m in Figure 7a, the linear MPC is slightly better.

(a) Prediction time = 6s, Optimization time = 3s

Energy Period (s)		6	7	8	9
Wave Height (m)	2.5	21.7	2.7	10.9	0.5
	2	45.4	27.0	13.8	7.9
	1.5	46.1	14.5	15.8	1.8
	1	19.6	17.3	9.6	5.6

(b) Prediction time = 6s, Optimization time = 6s

Energy Period (s)		6	7	8	9
Wave Height (m)	2.5	20.4	0.3	14.6	13.5
	2	-0.5	4.6	1.6	27.8
	1.5	0.6	3.9	3.7	21.8
	1	6.5	11.2	42.2	33.8

(c) Prediction time = 12s, Optimization time = 3s

Energy Period (s)		6	7	8	9
Wave Height (m)	2.5	45.7	13.8	9.0	6.7
	2	5.5	22.0	12.1	12.6
	1.5	18.7	4.5	15.2	10.3
	1	44.3	23.9	12.1	6.4

(d) Prediction time = 12s, Optimization time = 6s

Energy Period (s)		6	7	8	9
Wave Height (m)	2.5	32.8	59.8	6.6	19.6
	2	24.7	53.5	16.5	23.3
	1.5	34.2	56.3	34.9	14.7
	1	67.5	36.8	61.3	20.1

Figure 7. Percentage power performance difference between linear and nonlinear MPC models for different prediction horizons T_h and optimization times T_{opt}. (**a**) T_h = 6 s and T_{opt} = 3 s, (**b**) T_h = 6 s and T_{opt} = 6 s, (**c**) T_h = 12 s and T_{opt} = 3 s, (**d**) T_h = 12s and T_{opt} = 6 s.

However, it is important to note that the linear MPC, while producing more power at higher wave periods, often fails to comply with displacement constraints. Figure 8 illustrates this issue, showing the displacement of the WEC and the PTO force with their respective constraints for a wave with an energy period T_p = 9 s and H_s = 1.5 m. In this scenario, although the linear model is slightly better than the NLMPC in power output, the WEC displacement frequently exceeds the constraint limits. This could potentially lead to system damage if not adjusted for real-world conditions.

The greater improvement in energy capture with the NLMPC at lower-energy-period waves is primarily due to the inherent inaccuracies of the linear predictive model. These waves are steeper than higher-period waves and cause substantial variations in the wetted surface area of the buoy. In contrast, at higher wave periods, the difference in power production between the linear and nonlinear models becomes negligible due to the slower nature of the waves. Additionally, at these high-period waves, the effectiveness of the MPC may diminish as the wave period exceeds the prediction horizon.

In the cases where the optimization time is extended to T_{opt} = 6 s, it can be observed that the power generated by the NLMPC is improved across all of the wave conditions. This improvement is more pronounced when the prediction horizon is set to T_h = 6 s at smaller wave heights and longer wave periods. The reduced performance difference at higher wave heights can be attributed to the linear model exceeding the displacement constraints, which leads to an increase in power generation.

A clear demonstration of the benefits of using the NLMPC is evident in the case of a long prediction horizon with a long re-optimization time, as shown in Figure 7c. In this scenario, the inaccuracies of the linear model become highly significant, justifying the computational complexity of employing a nonlinear MPC. As observed from the table, the nonlinear MPC enhances system performance substantially, with improvements ranging from 6.5% to 67.5%. These differences can be attributed to the accumulation of error over the extended prediction period of the linear model and the extended optimization time required to re-evaluate the system's states. Therefore, the nonlinear MPC's ability

to account for more complex system dynamics and provide more accurate predictions becomes critically important in such conditions, leading to significant performance gains.

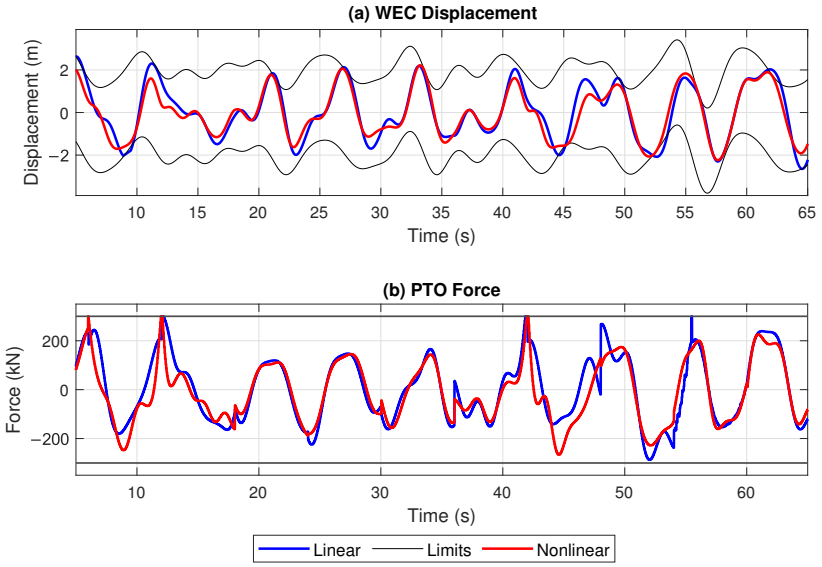

Figure 8. Displacement and PTO force for a wave of H_s = 2 m and T_p = 9 s. The prediction horizon and optimization time are 6 s and 3 s, respectively.

Furthermore, from Figure 7, it is shown that, overall, having a nonlinear model is beneficial in cases where the prediction horizons are kept the same while extending the optimization times. Being able to re-optimize less often increases the computational efficiency of the controller as it needs fewer optimizations. This could potentially compensate for having a more computationally demanding nonlinear model. However, this does not guarantee the generation of the highest amount of power. The following sections cover the differences in computation time and power generation across different controllers.

4.2. Computational Time

The plots in Figure 9 show the computational times for linear and nonlinear MPC to simulate 80 s of data. From these plots, it can be observed that the nonlinear MPC consistently exhibits higher computational times than the linear MPC across all conditions, which is expected as the nonlinear optimizations are more computationally complex to solve.

Overall, the computational time for both models increases with the wave height, but not significantly. Additionally, there is no consistent correlation between computational time and increasing wave periods, as trends vary depending on the prediction horizon and optimization time configuration. However, it is clear that increasing the prediction horizon and maintaining the same optimization time, as shown in plots (a) and (c), as well as (b) and (d), result in an average increase in computational time by factors of 2 and 3, respectively.

The comparison across different optimization times shows an increase in computational times on average of 2.4 times for the case of T_h = 6 s shown in plots (a) and (b), and 2 times for the case of T_h = 12 s as seen in plots (c) and (d). In addition, it can be observed that the difference in computations between the linear and nonlinear models becomes less pronounced as the optimization time increases, for instance, the case in the plot (b). Moreover, when the optimization time is extended from 3 to 6 s, both models exhibit a more flattened computational time profile, indicating stabilization in processing demands. This suggests that longer optimization periods might mitigate some of the computational inefficiencies of the nonlinear model, making it a more viable option under conditions where slightly delayed responses are permissible.

Although this paper does not focus on the real-time applicability of the controller, future research could explore optimization methods to reduce computational load and enable real-time applications. By implementing more efficient real-time MPC algorithms, the control system could become suitable for hardware testing environments, such as a low-friction testbed [32] or a WEC emulator [33]. Such setups would allow for an evaluation of the computational demands and performance of the control law under real-world conditions, potentially bridging the gap between theoretical models and practical, real-time applications.

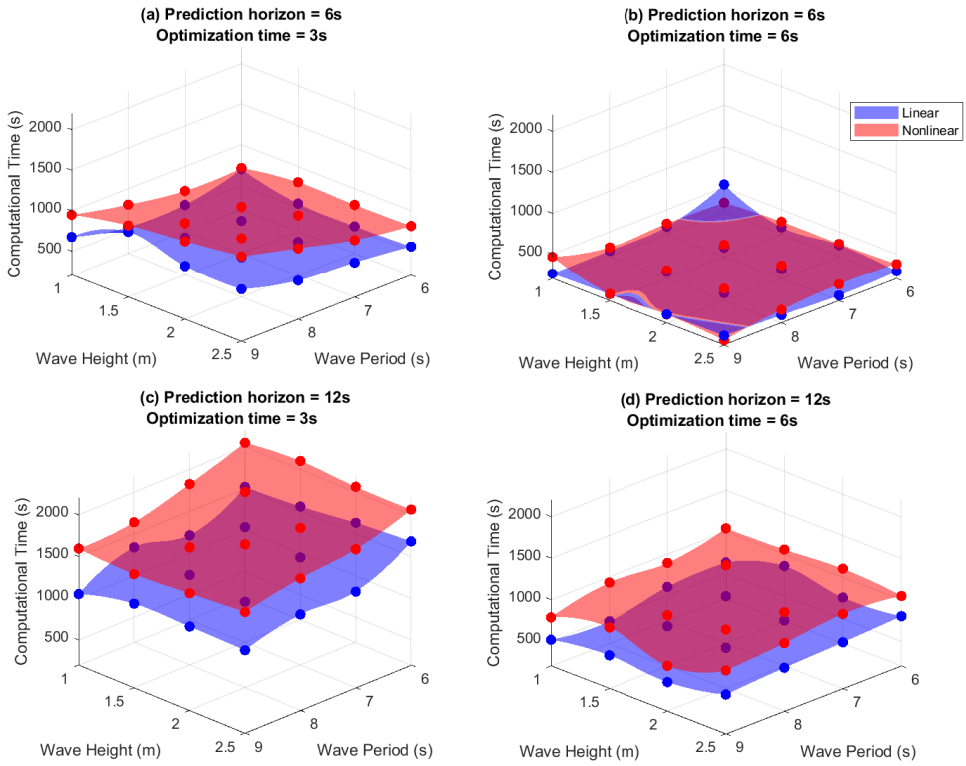

Figure 9. Computational time for different prediction horizons and optimization times for the linear and nonlinear MPC.

4.3. Power Generation

Utilizing the nonlinear MPC, the mean power absorbed for each control configuration was calculated and is presented in Figure 10. These data illustrate a clear pattern where shorter prediction horizons and optimization times are associated with higher power absorption. This observation aligns with findings from other studies. Bertsekas [34] notes that the prediction horizon T_h of the MPC should be determined experimentally to ensure the controller performs satisfactorily, but also points out that longer T_h values do not always correlate with higher efficiency. In the context of wave energy converters, the choice of T_h should consider the system's natural period [35] or the incoming wave period [36]. Sergiienko et al. [37] observed that increasing T_h from 1 to 5 s enhances power absorption; however, extending T_h from 6 to 16 s shows negligible impact on power generation. This suggests that in this case, a T_h of 6 s is optimal, balancing computational efficiency with effective power output.

The analysis of the power matrices also indicates that changes in optimization time (T_{opt}) significantly influence power absorption. For instance, reducing T_{opt} in the case of $T_h = 6$ increases the mean power absorbed by an average of 23%. While shorter optimization times lead to higher energy production, they also require greater computational demands. Similar to the impact of the prediction horizon on power production, decreasing T_{opt} does not necessarily result in higher power production, indicating the need to carefully consider these settings to optimize both power output and computational resources effectively.

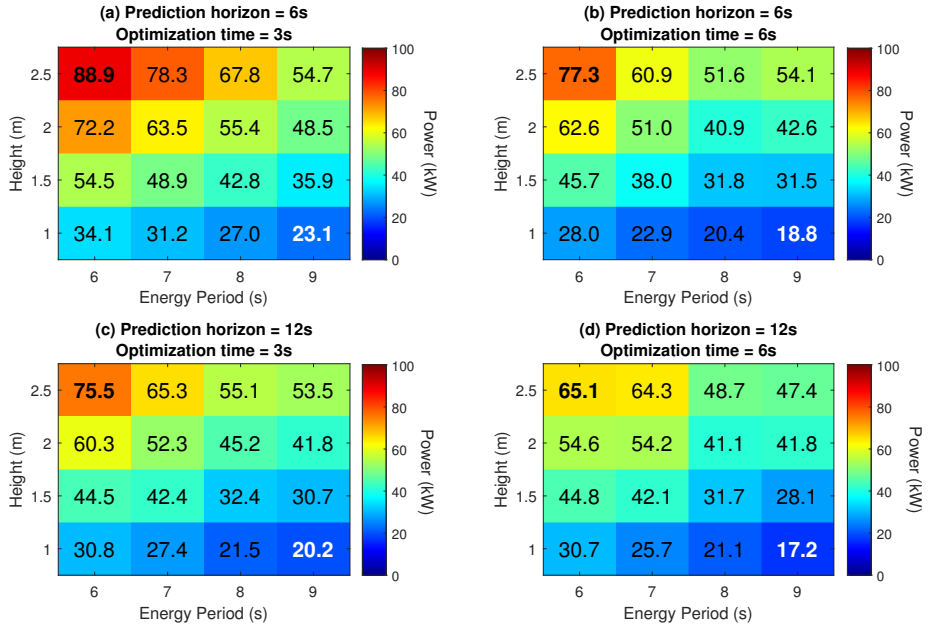

Figure 10. Mean power absorbed in (kW) for different NLMPC control configurations across a range of wave heights and wave periods.

5. Conclusions

The study effectively demonstrates the advantages of employing nonlinear model predictive control (NLMPC) over linear models in wave energy converters (WECs), particularly in optimizing power generation under various sea conditions. The nonlinear approach consistently outperforms its linear counterpart in power output, especially at lower wave periods with short optimization times, achieving improvements up to 44%. This increase in performance aligns with the objective of reducing the levelized cost of energy (LCOE) by enhancing the annual energy production (AEP) without significantly increasing operational or capital expenditures.

However, the findings also highlight a notable trade-off between computational efficiency and power optimization. While nonlinear models yield higher power outputs, they require longer computational times, especially as the optimization period is extended. This study shows that although extending the optimization time improves the power output across various wave conditions, it also leads to increased computational demands. Therefore, the choice between nonlinear and linear models and their respective settings must consider the specific operational priorities of a WEC project—whether the focus is on maximizing energy extraction or maintaining manageable computational loads.

In conclusion, advancing WEC technology with NLMPC offers a promising path toward optimizing power generation, albeit with considerations for computational demands. Future research should aim to refine these models by exploring optimization methods that can mitigate the computational burden of NLMPC, thereby making it more feasible for real-time applications. This balance between power efficiency and computational feasibility is essential to unlocking the full potential of WECs in renewable energy. Additionally, extending this analysis to incorporate PTO dynamics, PTO efficiency, and even a wave-to-wire framework could provide deeper insights into long-term system performance, including reductions in maintenance costs, fatigue analysis, and system durability. Another valuable avenue for exploration is evaluating optimal actuator sizing by analyzing the NLMPC's performance under varying saturation limits to ensure optimal energy absorption and actuator efficiency.

Author Contributions: Conceptualization, T.D.G., G.P., E.A. and H.Y.; methodology, T.D.G. and G.P.; software, T.D.G., G.P., E.A. and H.Y.; validation, T.D.G., G.P. and E.A.; formal analysis, T.D.G., G.P., E.A. and H.Y.; investigation, T.D.G. and G.P.; writing—original draft preparation, T.D.G.; writing—review and editing, G.P., E.A. and H.Y.; visualization, T.D.G.; supervision, G.P.; funding acquisition, G.P. All authors have read and agreed to the published version of the manuscript.

Funding: This research received no external funding.

Data Availability Statement: The original contributions presented in the study are included in the article, further inquiries can be directed to the corresponding author.

Conflicts of Interest: The authors declare no conflicts of interest.

Abbreviations

The following abbreviations are used in this manuscript:

AEP	Annual Energy Production
CAPEX	Capital Expenditures
FK	Froude–Krylov
HPA	Heaving Point Absorber
LCOE	Levelized Cost of Energy
LMPC	Linear Model Predictive Control
NLMPC	Nonlinear Model Predictive Control
OPEX	Operational Expenditures
PTO	Power Take-Off
WEC	Wave Energy Converter

References

1. Kilcher, L.; Fogarty, M.; Lawson, M. *Marine Energy in the United States: An Overview of Opportunities*; Technical Report NREL/TP–5700-78773 1766861; MainId:32690; National Renewable Energy Lab. (NREL): Golden, CO, USA, 2021. [CrossRef]
2. LiVecchi, A.; Copping, A.; Jenne, D.; Gorton, A.; Preus, R.; Gill, G.; Robichaud, R.; Green, R.; Geerlofs, S.; Gore, S.; et al. *Powering the Blue Economy: Exploring Opportunities for Marine Renewable Energy in Maritime Markets*; U.S. Department of Energy, Office of Energy Efficiency and Renewable Energy: Washington, DC, USA, 2019; pp. 158–163.
3. Chang, G.; Jones, C.A.; Roberts, J.D.; Neary, V.S. A comprehensive evaluation of factors affecting the levelized cost of wave energy conversion projects. *Renew. Energy* **2018**, *127*, 344–354. [CrossRef]
4. Wilson, D.; Bacelli, G.; Coe, R.; Bull, D.; Abdelkhalik, O.; Korde, U.; Robinett, R. *A Comparison of WEC Control Strategies*; Technical Report SAND2016–4293, 1431291, 639531; Sandia National Lab. (SNL-NM): Albuquerque, NM, USA, 2016. [CrossRef]
5. Falcão, A.F.d.O. Wave energy utilization: A review of the technologies. *Renew. Sustain. Energy Rev.* **2010**, *14*, 899–918. [CrossRef]
6. Drew, B.; Plummer, A.R.; Sahinkaya, M.N. A review of wave energy converter technology. *Proc. Inst. Mech. Eng. Part J. Power Energy* **2009**, *223*, 887–902. [CrossRef]
7. Cummins, W.; Navy, U.S. *The Impulse Response Functions and Ship Motions*; David Taylor Model Basin, United States Department of the Navy, David Taylor Model Basin: Carderock, MD, USA, 1962.
8. Perez, T.; Fossen, T.I. Time- vs. Frequency-domain Identification of Parametric Radiation Force Models for Marine Structures at Zero Speed. *Model. Identif. Control* **2008**, *29*, 1–19. [CrossRef]
9. Richalet, J.; Rault, A.; Testud, J.L.; Papon, J. Model predictive heuristic control: Applications to industrial processes. *Automatica* **1978**, *14*, 413–428. [CrossRef]
10. Ringwood, J.V.; Bacelli, G.; Fusco, F. Energy-Maximizing Control of Wave-Energy Converters: The Development of Control System Technology to Optimize Their Operation. *IEEE Control. Syst. Mag.* **2014**, *34*, 30–55. [CrossRef]
11. Faedo, N.; Olaya, S.; Ringwood, J.V. Optimal control, MPC and MPC-like algorithms for wave energy systems: An overview. *IFAC J. Syst. Control* **2017**, *1*, 37–56. [CrossRef]
12. Richter, M.; Magana, M.E.; Sawodny, O.; Brekken, T.K.A. Nonlinear Model Predictive Control of a Point Absorber Wave Energy Converter. *IEEE Trans. Sustain. Energy* **2013**, *4*, 118–126. [CrossRef]
13. Amann, K.U.; Magana, M.E.; Sawodny, O. Model Predictive Control of a Nonlinear 2-Body Point Absorber Wave Energy Converter with Estimated State Feedback. *IEEE Trans. Sustain. Energy* **2015**, *6*, 336–345. [CrossRef]
14. Giorgi, G.; Ringwood, J.V. Comparing nonlinear hydrodynamic forces in heaving point absorbers and oscillating wave surge converters. *J. Ocean Eng. Mar. Energy* **2018**, *4*, 25–35. [CrossRef]
15. Li, G. Nonlinear model predictive control of a wave energy converter based on differential flatness parameterisation. *Int. J. Control* **2017**, *90*, 68–77. [CrossRef]
16. Guerrero-Fernandez, J.L.; González-Villarreal, O.J.; Rossiter, J.A. Efficiency-aware nonlinear model-predictive control with real-time iteration scheme for wave energy converters. *Int. J. Control* **2023**, *96*, 1909–1921. [CrossRef]

17. Brekken, T.K. On Model Predictive Control for a point absorber Wave Energy Converter. In Proceedings of the 2011 IEEE Trondheim PowerTech, Trondheim, Norway, 19–23 June 2011; pp. 1–8. [CrossRef]
18. Fusco, F.; Ringwood, J.V. Short-Term Wave Forecasting for Real-Time Control of Wave Energy Converters. *IEEE Trans. Sustain. Energy* **2010**, *1*, 99–106. [CrossRef]
19. Anderlini, E.; Forehand, D.I.M.; Bannon, E.; Abusara, M. Reactive control of a wave energy converter using artificial neural networks. *Int. J. Mar. Energy* **2017**, *19*, 207–220. [CrossRef]
20. Demonte Gonzalez, T. Nonlinear Hydrodynamic Modeling and Control of Wave Energy Converters. Master's Thesis, Michigan Technological University, Houghton, MI, USA, 2024.
21. Falnes, J. *Ocean Waves and Oscillating Systems: Linear Interactions Including Wave-Energy Extraction*; Cambridge University Press: Cambridge, UK, 2002. [CrossRef]
22. Yassin, H.; Demonte Gonzalez, T.; Parker, G.; Wilson, D. Effect of the Dynamic Froude–Krylov Force on Energy Extraction from a Point Absorber Wave Energy Converter with an Hourglass-Shaped Buoy. *Appl. Sci.* **2023**, *13*, 4316. [CrossRef]
23. Dean, R.G.; Dalrymple, R.A. Water Wave Mechanics for Engineers and Scientists. In *Advanced Series on Ocean Engineering*; World Scientific Publishing: Singapore, 1991; Volume 2. [CrossRef]
24. Giorgi, G.; Ringwood, J.V. Computationally efficient nonlinear Froude–Krylov force calculations for heaving axisymmetric wave energy point absorbers. *J. Ocean Eng. Mar. Energy* **2017**, *3*, 21–33. [CrossRef]
25. Demonte Gonzalez, T.; Parker, G.G.; Anderlini, E.; Weaver, W.W. Sliding Mode Control of a Nonlinear Wave Energy Converter Model. *J. Mar. Sci. Eng.* **2021**, *9*, 951. [CrossRef]
26. Characterization of US. *Wave Energy Converter Test Sites: A Catalogue of Met-Ocean Data*; Sandia National Lab: Albuquerque, NM, USA, 2014.
27. Yu, Y.H.; Ruehl, K.; Van Rij, J.; Tom, N.; Forbush, D.; Ogden, D. WEC-Sim (Wave Energy Converter SIMulator)—WEC-Sim Documentation. Available online: http://wec-sim.github.io/WEC-Sim/main/index.html (accessed on 8 October 2024).
28. Pierson, W.J., Jr.; Moskowitz, L. A proposed spectral form for fully developed wind seas based on the similarity theory of S. A. Kitaigorodskii. *J. Geophys. Res. (1896–1977)* **1964**, *69*, 5181–5190. [CrossRef]
29. Faedo, N.; Pasta, E.; Carapellese, F.; Orlando, V.; Pizzirusso, D.; Basile, D.; Sirigu, S.A. Energy-maximising experimental control synthesis via impedance-matching for a multi degree-of-freedom wave energy converter. *IFAC-Papersonline* **2022**, *55*, 345–350. [CrossRef]
30. Findeisen, R.; Allgöwer, F. An Introduction to Nonlinear Model Predictive Control. In Proceedings of the 21st Benelux Meeting on Systems and Control, Mierlo, The Netherlands, 19–21 March 2002.
31. Rezaee, A. Controlling of Mobile Robot by Using of Predictive Controller. *IAES Int. J. Robot. Autom. (IJRA)* **2017**, *6*, 207–215. [CrossRef]
32. Van Wieren, M.; Gonzalez, T.D.; Yassin, H.; Jeanetta-Wark, N.; Kumpula, T.; Naglak, J.; Parker, G. Development of a Low-Friction Testbed for Model Scale Wave Energy Converter Control System Studies. In *The OCEANS 2023—MTS/IEEE U.S. Gulf Coast*; IEEE: Piscataway, NJ, USA, 2023; pp. 1–7, ISSN 0197-7385. [CrossRef]
33. Agyekum, E.B.; PraveenKumar, S.; Eliseev, A.; Velkin, V.I. Design and Construction of a Novel Simple and Low-Cost Test Bench Point-Absorber Wave Energy Converter Emulator System. *Inventions* **2021**, *6*, 20. [CrossRef]
34. Bertsekas, D. *Dynamic Programming and Optimal Control: Volume I*; Google-Books-ID: QVBEEAAAQBAJ; Athena Scientific: Nashua, NH, USA, 2012.
35. Hals, J.; Falnes, J.; Moan, T. Constrained Optimal Control of a Heaving Buoy Wave-Energy Converter. *J. Offshore Mech. Arct. Eng.* **2011**, *133*, 011401. [CrossRef]
36. Genest, R.; Ringwood, J.V. A critical comparison of model-predictive and pseudospectral control for wave energy devices. *J. Ocean Eng. Mar. Energy* **2016**, *2*, 485–499. [CrossRef]
37. Sergiienko, N.Y.; Cocho, M.; Cazzolato, B.S.; Pichard, A. Effect of a model predictive control on the design of a power take-off system for wave energy converters. *Appl. Ocean Res.* **2021**, *115*, 102836. [CrossRef]